

Electron-impact resonant vibrational excitation and dissociation processes involving vibrationally excited N₂ molecules

V. Laporta^{1,2,*}, D.A. Little², R. Celiberto^{3,1} and J. Tennyson²

¹ *Istituto di Metodologie Inorganiche e dei Plasmi, CNR, Bari, Italy*

² *Department of Physics and Astronomy,*

University College London, London WC1E 6BT UK and

³ *Dipartimento di Ingegneria Civile, Ambientale,
del Territorio, Edile e di Chimica, Politecnico di Bari, Italy*

Abstract

Resonant vibrational excitation cross sections and the corresponding rate coefficients for electron-N₂ collisions occurring through the N₂⁻(X ²Π_g) resonant state are reviewed. New calculations are performed using accurate potential energies curves for the N₂ electronic ground state, taken from literature, and for the N₂⁻ resonant state, obtained from *R*-matrix calculations. The calculations are extended to resonant excitation processes involving the N₂ ground state vibrational continuum, leading to dissociation. Electron impact dissociation is found to be significant from higher vibrational levels. Accurate analytical fits for the complete set of the rate coefficients are provided. The behavior of the dissociative cross sections is investigated for rotationally excited N₂ molecules, with $J = 50, 100$ and 150 and for different vibrational levels.

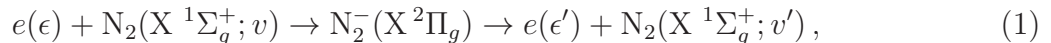
* vincenzo.laporta@ba.imip.cnr.it

I. INTRODUCTION

Nitrogen molecule plays a role of fundamental importance in many scientific and industrial activities. Typical examples are provided by air plasmas studied in a variety of fields such as environmental research, Earth's atmosphere phenomena, combustion, and aerospace technologies [1–4]. Detailed chemistries of processes involving molecular nitrogen have been prepared for such studies [5, 6].

One of the main aspects in the formulation of a model for non-equilibrium, nitrogen-containing plasmas is represented by the description of the vibrational kinetic and its role in redistributing the internal energy of the plasma among the atomic and molecular degrees of freedom. Electron-molecule collisions, involving vibrationally excited N_2 molecules and leading to vibrational excitations, represent a central process in the kinetic evolution of the plasma. In particular, resonant vibrational excitation (RVE) process, which occurs *via* the capture of the incident electron by the molecule with the formation of an unstable molecular anion, is one of the most important processes. In fact, decay of this resonance state can lead efficiently to single and multi-quantum vibrational excitations, which can strongly affect the vibrational population of the species in the plasma.

Several experimental [7–9] and theoretical [10–12] works have been devoted to study vibrational excitation of nitrogen by electron-impact. A complete set of cross sections and related rate coefficients, were recently reported in Ref. [13] (hereafter referred to as I), for the RVE process:



where the incident electron with energy ϵ is captured by the N_2 molecule, initially in its ground electronic state $X^1\Sigma_g^+$ and in the vibrational level v , with the formation of the resonant state $N_2^-(X^2\Pi_g)$ which decays into a free electron, with energy ϵ' , and a vibrationally excited molecule $N_2(X^1\Sigma_g^+; v')$. Cross sections $\sigma_{v,v'}(\epsilon)$ for process (1) were calculated in I using the so-called *local-complex-potential* (LCP) model for the scattering description, using Morse-like potential energies curves [14] as input parameters, for both $N_2(X^1\Sigma_g^+)$ and $N_2^-(X^2\Pi_g)$ states. The width for the $N_2^-(X^2\Pi_g)$ state was based on a semi-empirical analytical function optimized to reproduce the experimental data.

In this paper we provide new RVE cross section calculations for process (1) performed using an accurate potential curve for the N_2 molecule [15]. For the N_2^- ion, the potential

curve is obtained by *ab initio* calculations using the R -matrix method which also provides the resonance width as a function of the internuclear distance. The cross section calculations are extended to the RVE process ending in the vibrational continuum of the ground state [16]. The repulsive nature of the curve induces the separation of the nuclei so that the molecule undergoes dissociation with the production of two stable nitrogen atoms in their lowest electronic state. The resonant dissociation process can then be represented as:



This dissociative channel is particularly important in plasma kinetics because, in non-equilibrium conditions, it can compete with the dissociation from heavy species collisions [17–19].

The cross sections for processes (1) and (2) have been obtained as a function of the incident electron energy and for all the initial vibrational levels v by adopting the LCP model, and then used for the calculation of the corresponding rate coefficients, assuming a Maxwell distribution for electrons, according to the equation:

$$\kappa_{v,v'}(T) = \sqrt{\frac{8}{m_e \pi}} \left(\frac{1}{T}\right)^{3/2} \int_{\epsilon_{th}}^{\infty} d\epsilon \epsilon \cdot e^{-\frac{\epsilon}{T}} \cdot \sigma_{v,v'}(\epsilon), \quad (3)$$

where m_e is the electron mass and the temperature T is expressed in energy units. It worth be noted that Eq. (3) is no longer valid in non-equilibrium condition. Cross sections are also studied for some values of the rotational quantum number, namely $J = 50, 100$ and 150 .

The paper is organized as follows: in the next section the R -matrix calculations are described and the main equations of the LCP model are shown. The results are presented and commented in section III while, in section IV, a brief summary concludes the work.

II. THEORETICAL MODEL

A. R -matrix method

Electron- N_2 calculations were performed using the R -matrix method as implemented in the UKRMol codes [20]. For details of this methodology we refer to the review by one of us [21]. Put simply, the R -matrix method divides space into an inner region defined by a sphere centered on the target center-of-mass. This sphere, here taken to be $10 a_0$, is

assumed to enclose the entire charge cloud of the N -electron target. Within the sphere the wave function of the $(N+1)$ -electron scattering problem is built from target wave functions and extra functions designed to represent the scattering continuum. Here, and in general, this problem is built about using complete active space (CAS) configuration interaction (CI) representation of the target wave function for which a particularly efficient purpose-built algorithm is used [22]. In the outer region, the interaction of the scattering electron with the target is assumed to occur only *via* diagonal and off-diagonal multipole moments of the target. While the inner region problem only has to be solved once for each total scattering symmetry, the much faster outer region problem is solved at each scattering energy of interest. Below we give specific details for the present calculation.

Target calculations used the cc-pVQZ Gaussian Type Orbital (GTO) basis set due to Dunning. Orbitals for the N_2 target were generated using multi-configuration self-consistent field (MCSCF) calculations run in MOLPRO [23]. The CAS used in these calculations and to define the target wave function in the R -matrix calculations is given by:

$$(1\sigma_g, 1\sigma_u)^4(2\sigma_g, 2\sigma_u, 1\pi_u, 3\sigma_g, 1\pi_g, 3\sigma_u)^{10}.$$

A total of 128 target states were generated (eight per symmetry) of which the lowest 49 in energy were retained for the inner region calculation. Calculations were performed for a 100 geometries from 0.8 Å to 3.77 Å in steps of 0.03 Å.

For the scattering calculations, $(4\sigma_g, 5\sigma_g, 4\sigma_u, 2\pi_u, 2\pi_g, 1\delta_g)$ target orbitals were retained. These were augmented by continuum orbital containing up to g ($l = 4$) functions represented by a GTO expansion at the target center-of-mass [24]. These were orthogonalized to the target orbitals with a deletion threshold set to 10^{-7} [25]. The target times continuum configurations were augmented by the following short-range functions based on the use of target orbitals:

$$(1\sigma_g, 1\sigma_u)^4(2\sigma_g, 2\sigma_u, 1\pi_u, 3\sigma_g, 1\pi_g, 3\sigma_u)^{11},$$

which involves placing the scattering electron in the target CAS, and

$$(1\sigma_g, 1\sigma_u)^4(2\sigma_g, 2\sigma_u, 1\pi_u, 3\sigma_g, 1\pi_g, 3\sigma_u)^{10}(2\pi_u, 4\sigma_g, 5\sigma_g, 2\pi_g, 1\delta_g, 4\sigma_u)^1,$$

where the scattering electron enters and otherwise unoccupied target virtual. These configurations were not constrained by contracting to target CI wave functions [26].

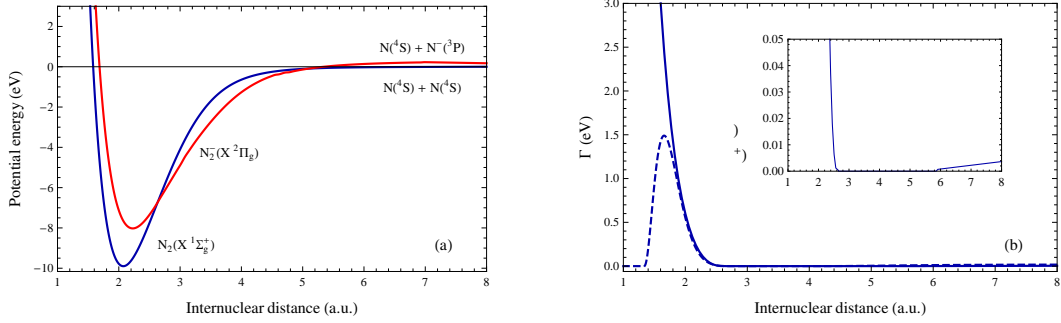


FIG. 1: (a) Potential energy curves for $N_2(X^1\Sigma_g^+)$ and $N_2^-(X^2\Pi_g)$ and (b) resonance width $\Gamma(R)$ as a function of the internuclear distance: solid line, this work; dashed line, phenomenological width calculated in I. The inset plot shows a magnified view of our resonance width ($\Gamma(R) \leq 0.05$ eV).

For computational efficiency, only the lowest two target states, $X^1\Sigma_g^+$ and $A^3\Sigma_u^+$, were retained in the outer region calculation. This problem was solved by propagating the R -matrix to $100.1 a_0$ and then using a Gailitis expansion. The resulting eigenphases were searched for a resonance which was fitted to a Breit-Wigner form using an automated procedure [27]. These calculations concentrated on the $^2\Pi_g$ total symmetry as this is the symmetry of the well known, low-lying N_2^- shape resonance.

The $N_2(X^1\Sigma_g^+)$ potential energy curve is taken from Le Roy *et al.* [15] who obtained it by an accurate fit to spectroscopic data. The resulting potential curves for both N_2 and N_2^- , along with the corresponding width $\Gamma(R)$, are shown in Fig. 1(a)-(b) respectively. The $N_2^-(X^2\Pi_g)$ resonance curve crosses $N_2(X^1\Sigma_g^+)$ at $\sim 2.657 a_0$ and $\sim 5.132 a_0$. In this intermediate region the molecular ion N_2^- becomes stable and the resonance width vanishes, as is shown in the inset box in Fig. 1(b). For geometries where N_2^- is bound, the position of the bound state was determined using the same model and by performing negative energy scattering calculations [28]. Table I reports some relevant spectroscopical parameters for the two potentials.

	$\text{N}_2(\text{X } ^1\Sigma_g^+)$	$\text{N}_2^-(\text{X } ^2\Pi_g)$
R_e (a ₀)	2.07	2.23
D_e (eV)	9.89	8.22
T_e (eV)	0	1.97
RP (eV)	–	2.34
EA (eV)	–	– 0.30

TABLE I: Equilibrium distance (R_e), dissociation energy (D_e), vertical excitation (T_e), resonance position calculated at the N_2 equilibrium bond-length (RP) and electronic affinity (EA) for the N_2 and N_2^- ground state potential energy curves.

B. Vibrational dynamics

In this section the main equations for the description of the vibrational dynamics of the collision in the framework of the LCP model are summarized. Extensive theoretical formulations of electron-molecule resonant scattering can be found elsewhere [29–31].

The cross sections for the RVE processes in (1), with incoming electron energy ϵ , were calculated using the following formula:

$$\sigma_{v,v'}(\epsilon) = g \frac{64 \pi^5 m^2}{\hbar^4} \frac{k'}{k} |\mathcal{T}_{v,v'}(\epsilon)|^2, \quad (4)$$

where $k(k')$ is the ingoing (outgoing) electron momentum, g contains the spin-statistic weight factors and $v(v')$ represents the bound initial (final) nitrogen vibrational levels. $\mathcal{T}_{v,v'}$ is the T -matrix of the process. The definition in Eq. (4) can be extended to the resonant dissociation process (2), by considering that the final vibrational energy falls now in the continuum spectrum of the N_2 ground state potential. The right-hand side of Eq. (4) retains the same form but it expresses now the energy-differential cross section $d\sigma_{v,\epsilon'}(\epsilon)/d\epsilon'$. An extra integration over the final continuum levels of energy ϵ' is thus required according to [16, 32, 33]:

$$\sigma_v(\epsilon) = \int_{\epsilon_{th}}^{\epsilon_{max}} d\epsilon' \frac{d\sigma_{v,\epsilon'}(\epsilon)}{d\epsilon'}, \quad (5)$$

where ϵ_{th} is the dissociation threshold. In our calculations the integration over the continuum has been extended up to $\epsilon_{max} = \epsilon_{th} + 10$ eV.

According to the LCP model of Fano-Bardsley's theory of resonant scattering [29, 34] the

\mathcal{T} -matrix in Eq. (4) is given by:

$$\mathcal{T}_{v,v'}(\epsilon) = \langle \chi_{v'} | V_{dk} | \xi \rangle, \quad (6)$$

where $\xi(R)$ is the resonant state nuclear wave function, solution of the Schrodinger-like equation

$$(T_N + V^- - \frac{i}{2}\Gamma - E)\xi(R) = -V_{dk} \chi_v, \quad (7)$$

with total energy $E = \epsilon + \epsilon_v$ and for the resonant complex potential $(V^-(R), \Gamma(R))$. Moreover, $\chi_{v(v')}(R)$ is the initial (final) vibrational wave function, with the corresponding eigenvalues $\epsilon_{v(v')}$, belonging to the N_2 ground state potential energy, denoted by $V^0(R)$, and T_N is the nuclear operator. Finally, V_{dk} is the continuum-discrete coupling potential given by,

$$V_{dk} = \sqrt{\frac{1}{4\pi} \frac{\Gamma(R)}{2\pi} \frac{\hbar^2}{m k(R)}}, \quad (8)$$

where $k(R) = \sqrt{2m [V^-(R) - V^0(R)]/\hbar}$.

III. RESULTS AND DISCUSSION

The potential curve for the N_2 ground state, used in the present calculations, supports 59 vibrational levels, which are reported in Table II. This is fewer than the 68 levels found for the Morse curve adopted in I, which implies that there is not a one-to-one correspondence in the energy eigenvalues for the same v in the two sets of calculations. However, the energies of the first few levels do not show large differences compared with those of I and so the updated cross sections remain practically the same. This means that the good agreement between the calculated cross sections with the experimental measurements observed in I is retained in the present results, as can be seen in Figs. 2 and 3 where the new theoretical results are compared with the experimental data of Allan [7] and Vičić *et al.* [8] respectively.

Figure 4 compares also the calculated total cross sections with the experimental data of Refs. [35, 36]. Our theoretical curve was obtained as a sum over the final vibrational resonant cross sections, in the resonance region (~ 2 eV), and the non-resonant background contribution $\sigma^{bg}(\epsilon)$, as:

$$\sigma^{tot}(\epsilon) = \sum_{v'} \sigma_{0 \rightarrow v'}^{res}(\epsilon) + \sigma^{bg}(\epsilon), \quad (9)$$

v	ϵ_v (eV)						
0	0.000	15	3.959	30	7.084	45	9.163
1	0.288	16	4.195	31	7.260	46	9.252
2	0.573	17	4.426	32	7.430	47	9.335
3	0.855	18	4.654	33	7.596	48	9.409
4	1.133	19	4.878	34	7.757	49	9.476
5	1.408	20	5.099	35	7.913	50	9.535
6	1.679	21	5.315	36	8.064	51	9.587
7	1.947	22	5.528	37	8.210	52	9.631
8	2.211	23	5.737	38	8.350	53	9.667
9	2.471	24	5.942	39	8.485	54	9.696
10	2.728	25	6.143	40	8.614	55	9.717
11	2.982	26	6.339	41	8.737	56	9.732
12	3.232	27	6.532	42	8.853	57	9.742
13	3.478	28	6.721	43	8.963	58	9.748
14	3.720	29	6.905	44	9.067		

TABLE II: Vibrational levels given by the N_2 potential energy curve [15] counted from the lowest level $v = 0$, which has a zero point energy of 0.146 eV.

where $\sigma^{bg}(\epsilon)$ was calculated using the R -matrix method to evaluating the T -matrix at the equilibrium internuclear distance for all symmetries except the resonant $^2\Pi_g$ one. Above ~ 2.5 eV our cross sections are in good agreement with the observed ones. At lower energies the background is too high. This is due to the lack of polarization effects in the R -matrix calculation which become increasingly important at very low collision energies. It is possible to include these effects in the calculation but only by making the calculation significantly more expensive [37]. In the resonance region below ~ 2.5 eV, the theoretical peaks are higher than the experimental ones and show a small shift which is, however, not present in the comparison with the inelastic cases shown in Figs. 2 and 3.

There is an important difference between the resonance widths shown in Fig. 1(b). The width calculated *ab initio* using the R -matrix method (solid line), shows a monotonic in-

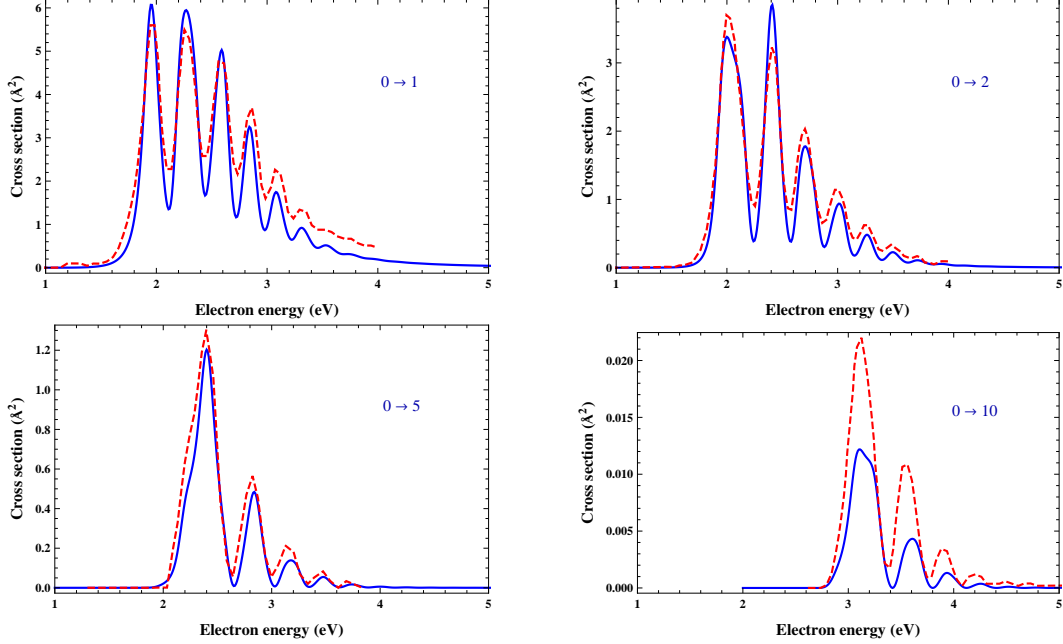


FIG. 2: Cross section comparison between the present calculations (full-blue line) and the measurements (dashed-red line) of Allan [7]. The experimental data have an estimated uncertainty of $\pm 20\%$.

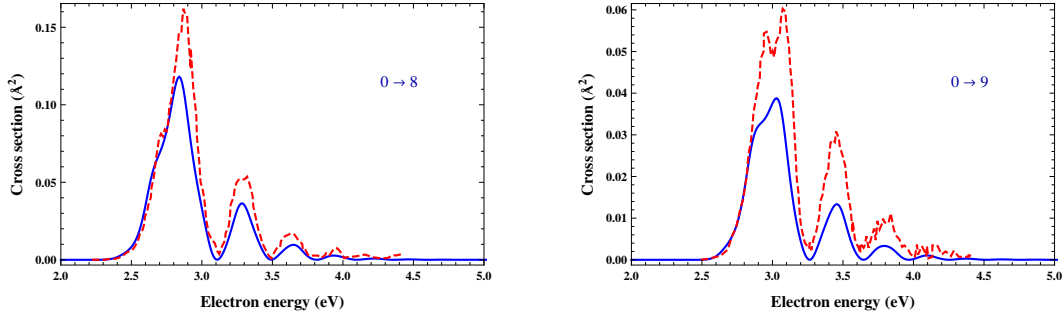


FIG. 3: Cross section comparison between the present calculations (full-blue line) and the measurements of Vicić *et al.* [8].

crease toward short bond-lengths which contrasts with the bell-shaped behavior of the semi-empirical $\Gamma(R)$ obtained in I (dashed line). However, the two curves overlap for bond-lengths greater than $1.8 a_0$, which covers the Franck-Condon region for the transitions from the vibrational ground state. This explains the absence of any substantial differences between the present calculations and those reported in I for the corresponding vibrational excitation cross sections.

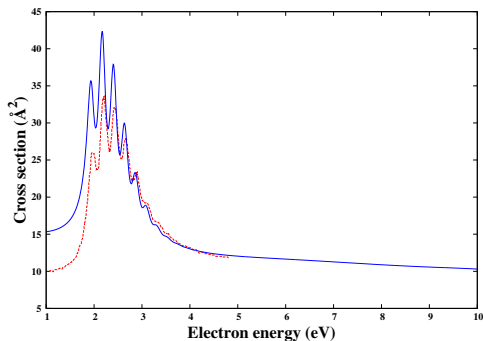


FIG. 4: Comparison between calculated and measured total cross sections (see text). Present theoretical results (full-blue line) and experimental data (dashed-red line) [35, 36].

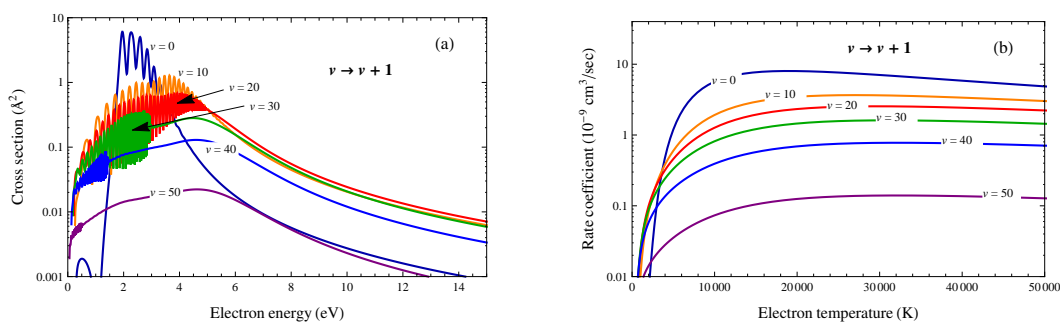


FIG. 5: (a) electron- N_2 resonant vibrational-excitation cross sections and (b) corresponding rate coefficients for selected single-quantum transitions.

Figure 5 shows a set of the new calculated RVE cross sections and the corresponding rate coefficients for the $v \rightarrow v + 1$ single-quantum transitions, which play a prominent role in the plasma vibrational kinetic. The cross section curves displayed are labeled with the selected values of the vibrational quantum number v . As extensively discussed in paper I the sharp peaks in the cross sections shown in Figs. 2–5 are due to the well know boomerang-oscillations and their position corresponds to the energy of the resonant vibrational levels. For high energies the cross sections drop down of several orders of magnitude, relative to their peak value, so that in the integration of the rate coefficients in Eq. (3) they were considered negligible beyond 15 eV.

The cross sections for the dissociative process (2), calculated by Eq. (5), are shown in Fig. 6 for some initial vibrational levels as a function of the incident electron energy. An immediate result which can be drawn from Fig. 6a, where the plots are represented in

log y -scale, is that the cross sections for low levels ($v \lesssim 20$) are extremely small, so that the role of the corresponding dissociative processes in plasma kinetics can be expected to be negligible. For higher levels however, the cross sections tend to saturate above 10^{-2} \AA^2 , which implies that in strong non-equilibrium plasma conditions, that is when the higher levels are overpopulated with respect to the Boltzmann distribution, the dissociative processes, starting from these levels, will play a major role. Figure 6b shows the cross sections on a linear scale for some v values ranging from 0 through 30. All the curves exhibit two large, sharp peaks and a structure of smaller intensity very close to the apparent threshold. These features are also present in all the calculated cross sections as can be seen in Fig. 6c. Inspection of the numerical values shows that the peak positions coincide with some of the vibrational eigenvalues of the $\text{N}_2^-(X^2\Pi_g)$ resonant state, placed inside the electronic affinity gap, of $|0.30| \text{ eV}$ (see Table I), between the asymptotic limits of the $\text{N}_2(X^1\Sigma_g)$ and $\text{N}_2^-(X^2\Pi_g)$ potential curves. In this interval we found twelve resonant vibrational levels which are the only “bound” states that can lead to dissociation. These levels, in fact, can enter in resonance with the continuum of the N_2 ground state while above the N_2^- dissociation limit, instead, the interaction of the two continua occurs.

As v is increased the threshold of the resonant dissociation process is lowered so that the cross section peaks in Fig. 6b move toward lower energies. On the other side of the peaks and for large incident energies, some oscillation is observed in the curves. This is due to numerical noise. In fact, the very small absolute values of the low-level cross sections ($\sim 10^{-8} \text{ \AA}^2$) implies a reduced accuracy in the calculations so that numerical instabilities become evident. For $v = 8, 9, 10$ the corresponding cross sections ($\sim 10^{-7} \text{ \AA}^2$, not shown) are even larger while for $v \gtrsim 20$, for which the cross sections become significantly large, the oscillations remain confined to very small values and disappear from the plots.

Figure 6c shows cross sections for some initial levels with $v \geq 35$; besides the sharp peaks already discussed, there is also a broad maximum arising about 5 eV, whose intensity grows with the vibrational quantum number up to $v = 50$ then decreases for $v = 53$ and 55 (dashed lines). This maximum occurs when the N_2 vibrational states lie in the continuum spectrum of N_2^- ion and is therefore due to the interplay of the Franck-Condon overlap between the N_2 and N_2^- bound and continuum levels respectively, during the electron capture, and that of the two continua in the emission process.

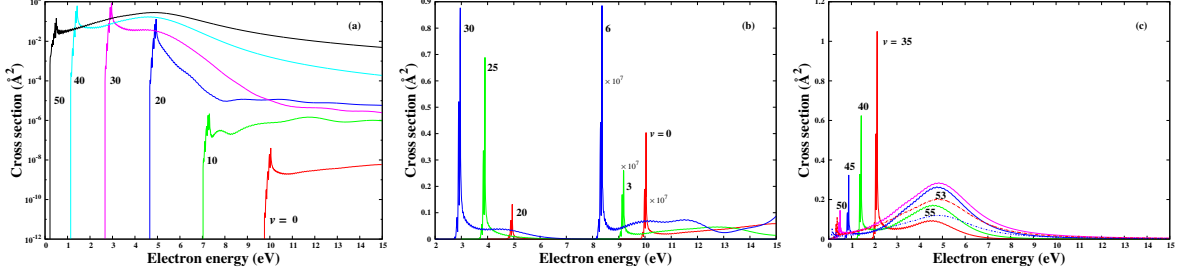


FIG. 6: Resonant electron- N_2 dissociation cross sections for some initial vibrational levels, as indicated in the figure, and for $J = 0$. Panel (a) gives plots on a log y -scale. In panel (b) the cross sections for $v = 0, 3$ and 6 have been multiplied by 10^7 , as shown. In panel (c) the dashed lines ($v = 53$ and 55) indicate a decreasing trend for the corresponding cross sections.

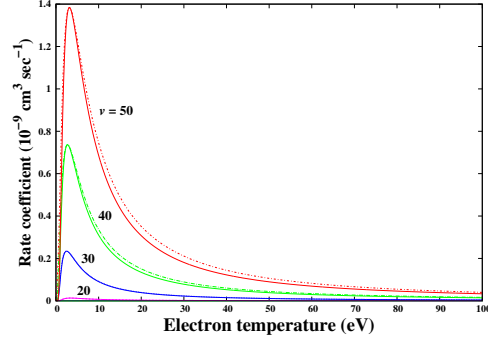


FIG. 7: Calculated (full lines) and fitted (dashed lines) rate coefficients for resonant dissociation as a function of the electron temperature and for the indicated vibrational levels.

Rate coefficients were also calculated for process (2) using Eq. (3) and the corresponding dissociative cross sections. Figure 7 shows the rates as a function of the electron temperature for the initial vibrational levels $v = 20, 30, 40$ and 50 . These rates follow the same trend as the cross sections, being negligible for low v ($\lesssim 20$) and becoming significant for higher vibrational levels. Likely in the RVE case, the dissociation cross sections decrease rapidly as a function of the electron energy, so again we extended the integration in the calculation of the rate coefficients up to 15 eV.

The rates can be easily and accurately reproduced using the following analytical expression:

$$\kappa_v(T) = \kappa_v^{max} \left(\frac{T^{max}}{T} \right)^{3/2} e^{-\frac{T^{max}}{T}}, \quad (10)$$

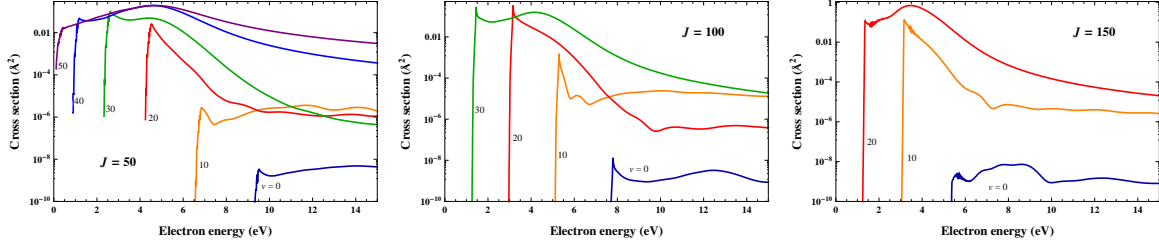


FIG. 8: Resonant dissociation cross sections as a function of the electron energy, for some vibrational levels and for $J = 50$, $J = 100$ and $J = 150$.

already successfully tested for electron- H_2 scattering [38]. The equation requires only two parameters, T_v^{max} and κ_v^{max} , which are the coordinates of the maximum value of the calculated rates for each level v . Eq. (10) works quite well for all v but the last three values ($v = 56, 57$ and 58) as the corresponding rates show some irregularity, probably coming from the related cross sections which, for these very high levels, suffer from reduced numerical accuracy. T_v^{max} and κ_v^{max} are provided here as a supplementary material for both dissociative ($0 \leq v \leq 55$) and RVE processes ($0 \leq v \leq v' \leq 55$). The RVE rates for $v \geq v'$ can be obtained by detailed balance [39].

We also investigated the behavior of the dissociative process as a function of rotational state. Figure 8 shows the cross sections for $J = 50, 100$ and 150 and for different v . In calculating these cross sections we have started the integration in Eq. (5) above the centrifugal barrier created in the N_2 potential curve by the nuclear rotation, instead of from the dissociation energy ϵ_{th} . This barrier, in fact, can support a number of quasi-bound states which can lead to dissociation by tunneling. We have assumed that the contribution of these metastable states, if they exist, to dissociation is small compared to the process occurring from the repulsive part of the potential curve, due to the delay accumulated by the nuclei inside the barrier. Figure 8 shows, for a given J , that again the cross sections present structures near the threshold and become of significant values for high vibrational levels, comparable in magnitude with those for $J = 0$.

IV. CONCLUSIONS

In this article we update the resonant vibrational excitation cross sections and rate coefficients reported in I. Our new calculations use accurate potential energies for both N_2 and N_2^- ground states. For the neutral molecule we use the experimentally-derived potential curves [15], while for N_2^- resonant state we perform new calculations using the R -matrix method, obtaining also the resonance width as a function of the bond length.

We extend the cross section calculations to the study of dissociative resonant vibrational excitations using the same model. The energy-dependent cross section curves obtained show some sharp peaks close to the process threshold, which are caused by resonant bound states located in between the dissociation limits of the N_2 and N_2^- molecules. Above these levels resonant coupling occurs among the two continua of the neutral and ionic species. The dissociation cross sections are of very small values for low initial vibrational levels, but become important for high v ($\gtrsim 20$). The same behavior is shown by the corresponding rate coefficients. For these last quantities, as well as for the RVE rates, a two-parameter analytical fitting expression has been formulated for their rapid and accurate evaluation which should be useful for practical applications. Finally, cross sections for $J = 50, 100$ and 150 , and for different v have been also investigated. Their behavior, as well as their order of magnitude, is comparable to the cross sections for $J = 0$.

As already stressed previously, the resonant dissociative cross sections starting from $v = 0$ level is particularly small. This can be better seen in comparison with the experimental measurements of $\text{N}_2(v = 0)$ reported by Cosby [40] which found that the dominant contribution to dissociation comes from electronically excited states leading to $\text{N}(^2D) + \text{N}(^4S)$. However, in nitrogen plasmas, exposed to high temperature and electric fields, the contribution coming from the resonant dissociation from all the vibrational levels, is comparable with the dominant kinetic mechanism of dissociation induced by vibrational quanta exchange, which gradually excite the molecules up to the vibrational continuum (the so-called ‘*pure-vibrational mechanism*’) as discussed in Ref. [41].

The complete set of cross sections and the corresponding rate constants can be downloaded from the ‘Phys4Entry’ database [42] and the parameters of the fit in Eq. (10) can be found as supplementary material of this paper.

Acknowledgements

This work received funding from the European Community's Seventh Framework Programme (FP7/2007-2013) under grant agreement n. 242311. One of the authors (DAL) would like to also thank support from Themisys Limited for supporting a studentship. The authors wish to thank Drs. W.M. Huo, R. Jaffe and D.W. Schwenke (NASA Ames Research Center) for providing the N_2 potential energy curve in Ref. [15].

References

- [1] F. J. Gordillo-Vázquez. *J. Phys. D: Appl. Phys.*, 41:234016, 2008.
- [2] J.S. Shang and S.T. Surzhikov. *Prog. Aerospace Sci.*, 53:46, 2012.
- [3] V. Laporta and D. Bruno. *J. Chem. Phys.*, 138::104319, 2013.
- [4] M. Capitelli, R. Celiberto, G. Colonna, V. Laporta, and J. Tennyson. In *International Conference on Phenomena in Ionized Gases (XXXI ICPIG). Granada (ES)*, 14-19 July, 2013.
- [5] A. Bultel and J. Annaloro. *Plasma Sources Sci. Technol.*, 22:025008, 2013.
- [6] O. Dutuit, N. Carrasco, R. Thissen, V. Vuitton, C. Alcaraz, P. Pernot, N. Balucani, P. Casavecchia, A. Canosa, S. Le Picard, J.-C. Loison, Z. Herman, J. Zabka, D. Ascenzi, P. Tosi, P. Franceschi, S. D. Price and P. Lavva, *Astrophys. J. Suppl.*, 204:20, 2013
- [7] M. Allan. *J. Phys. B: At. Mol. Opt. Phys.*, 18:4511, 1985.
- [8] M Vacic, G Poparic, and D S Belic. *J. Phys. B: At. Mol. Opt. Phys.*, 29:1273, 1996.
- [9] M. Ristic, G.B. Poparic, and D.S. Belic. *Chem. Phys.*, 331:410 – 416, 2007.
- [10] B. I. Schneider, M. Le Dourneuf, and Vo Ky Lan. *Phys. Rev. Lett.*, 43:1926–1929, Dec 1979.
- [11] Winifred M. Huo, Thomas L. Gibson, Marco A. P. Lima, and Vincent McKoy. *Phys. Rev. A*, 36:1632–1641, Aug 1987.
- [12] A A Mihajlov, V D Stojanovic, and Z Lj Petrovic. *J. Phys. D: Appl. Phys.*, 32:2620, 1999.
- [13] V. Laporta, R. Celiberto, and J. M. Wadehra. *Plasma Sources Sci. Technol.*, 21:055018, 2012.
- [14] F. R. Gilmore. *J. Quant. Spectrosc. Radiat. Transf.*, 5:369 – 89, 1965.
- [15] R. J. Le Roy, Y. Huang, and C. Jary. *J. Chem. Phys.* 125:164310, 2006.

- [16] D. E. Atems and J. M. Wadehra. *J. Phys. B: At. Mol. Opt. Phys.*, 26:L759, 1993.
- [17] M. Panesi, R. L. Jaffe, D. W. Schwenke, and T. E. Magin. *J. Chem. Phys.*, 138:044312, 2013.
- [18] F. Esposito, I. Armenise, and M. Capitelli. *Chem. Phys.*, 331:1 – 8, 2006.
- [19] Igor V. Adamovich. *Phys. Fluids*, 26:046102, 2014.
- [20] J. M. Carr, P. G. Galiatsatos, J. D. Gorfinkiel, A. G. Harvey, M. A. Lysaght, D. Madden, Z. Masin, M. Plummer, and J. Tennyson. *Eur. Phys. J. D*, 66:58, 2012.
- [21] J. Tennyson. *Phys. Rep.*, 491:29 – 76, 2010.
- [22] J. Tennyson. *J. Phys. B: At. Mol. Opt. Phys.*, 29:1817–1828, 1996.
- [23] H.-J. Werner, P. J. Knowles, G. Knizia, F. R. Manby, M. Schütz, et al. MOLPRO, version 2010.1, a package of ab initio programs, 2010.
- [24] A. Faure, J. D. Gorfinkiel, L. A. Morgan, and J. Tennyson. *Comput. Phys. Commun.*, 144: 224–241, 2002.
- [25] L. A. Morgan, J. Tennyson, and C. J. Gillan. *Comput. Phys. Commun.*, 114:120 – 8, 1998.
- [26] J. Tennyson. *J. Phys. B: At. Mol. Opt. Phys.*, 29:6185–6201, 1996.
- [27] J. Tennyson and C. J. Noble. *Comput. Phys. Commun.*, 33:421 – 4, 1984.
- [28] B. K. Sarpal, S. E. Branchett, J. Tennyson, and L. A. Morgan. *J. Phys. B: At. Mol. Opt. Phys.*, 24:3685–99, 1991.
- [29] J. N. Bardsley and F. Mandl. *Rep. Prog. Phys.*, 31:471, 1968.
- [30] W. Domcke. *Phys. Rep.*, 208:97 – 188, 1991.
- [31] J. M. Wadehra. in *Nonequilibrium Vibrational Kinetics. Edited by M. Capitelli, University of Bari, Italy (Topics in Current Physics, Vol. 39, Springer-Verlag 1986.)*, 1986.
- [32] D. T. Stibbe and J. Tennyson. *New J. Phys.*, 1:2, 1998.
- [33] R. Celiberto, A. Laricchiuta, U. T. Lamanna, R. K. Janev, and M. Capitelli. *Phys. Rev.*, 60: 2091 – 2103, 1999.
- [34] J. N. Bardsley. *J. Phys. B: At. Mol. Phys.*, 1:349, 1968.
- [35] R. E. Kennerly. *Phys. Rev. A*, 21:1876, 1980.
- [36] Y. Itikawa. *J. Phys. Chem. Ref. Data*, 35:31, 2006.
- [37] W. J. Brigg, J. Tennyson and M. Plummer. *J. Phys. B: At. Mol. Opt. Phys.*, submitted, 2014.
- [38] R. Celiberto, R. K. Janev, V. Laporta, J. Tennyson, and J. M. Wadehra. *Phys Rev A*, 88: 062701, 2013.
- [39] R. Celiberto, R. K. Janev, and D. Reiter. *Plasma Phys. Control. Fusion*, 54:035012, 2012.

- [40] P. C. Cosby. *J. Chem. Phys.*, 98:9544, 1993.
- [41] M. Capitelli, G. Colonna, G. D'Ammando, V. Laporta, and A. Laricchiuta *Chem. Phys.*, in press, 2014.
- [42] Database of the european union phys4entry project, 2012.
<http://users.ba.cnr.it/imip/cscpal38/phys4entry/database.html>